

# Weight Equalizing Shift Scaler-Coupled Post-training Quantization

Jihun Oh, SangJeong Lee, Meejeong Park, Pooni Walagaurav, Kiseok Kwon

Samsung Research, Samsung Electronics Co.  
33, Seongchon-gil, Seocho-gu, Seoul, 06765, Republic of Korea  
{jihun2331.oh, sj94.lee, mia.park, pt.gaurav, kiseok.kwon}@samsung.com

## Abstract

Post-training, layer-wise quantization is preferable because it is free from retraining and is hardware-friendly. Nevertheless, accuracy degradation has occurred when a neural network model has a big difference of per-out-channel weight ranges. In particular, the MobileNet family has a tragedy drop in top-1 accuracy from 70.60%  $\sim$  71.87% to 0.1% on the ImageNet dataset after 8-bit weight quantization. To mitigate this significant accuracy reduction, we propose a new weight equalizing shift scaler, i.e. rescaling the weight range per channel by a 4-bit binary shift, prior to a layer-wise quantization. To recover the original output range, inverse binary shifting is efficiently fused to the existing per-layer scale compounding in the fixed-computing convolutional operator of the custom neural processing unit. The binary shift is a key feature of our algorithm, which significantly improved the accuracy performance without impeding the memory footprint. As a result, our proposed method achieved a top-1 accuracy of 69.78%  $\sim$  70.96% in MobileNets and showed robust performance in varying network models and tasks, which is competitive to channel-wise quantization results.

## Introduction

Quantization involves mapping continuous real values to discrete integers, which is demanding to reduce the computational and memory costs. Inference using quantized weights and feature maps in fixed-precision (e.g., 8 bits) can compute many operations per second and reduce memory bandwidth and power consumption. In detail, the chip area of a multiplier is proportional to the square of precision so low precision-based computing can lead to either a reduction in chip area or an increase in computing capability under the same chip area. Also, the energy consumption of 8-bit multiplier and adder is 18 x and 30 x lower than 32-bit floating-point, respectively (Horowitz 2014). Therefore, quantization is necessary for deep learning models to run on energy-efficient specialized hardware such as neural processing units (NPU) (Chen, Emer, and Sze 2016; Judd et al. 2016; Albericio et al. 2017; Jouppe et al. 2017; Lee et al. 2018; Zhao et al. 2019b).

According to the intervention point of quantization, there are two forms: quantization-aware training (QAT) and post-training quantization (PTQ). In detail, QAT (Han, Mao, and Dally 2015; Courbariaux, Bengio, and David 2015; Hubara et al. 2016; Lee, Kapoor, and Kim 2018; Jung et al. 2019)

is to simulate quantization during the time of training from scratch or fine-tuning, enabling to apply the effect of quantization simultaneously. Training can compensate for accuracy degradation due to quantization so we can reach even lower precision such as 4 bits. However, QAT is not always available in real practice because it requires large training or validation dataset with label information and complicated training settings, and takes a lot of time to get results.

Alternatively, PTQ (Krishnamoorthi 2018; Nagel et al. 2019; Banner, Nahshan, and Soudry 2019; Zhao et al. 2019a; Cai et al. 2020) can quantize pre-trained models in a single shot and is free from large training and validation datasets, but just small representative dataset without labels for activation quantization. It is simple and fast because of unnecessary of retraining. Nevertheless, quantizing full precision models into fixed point without retraining in PTQ yields quantization error on weights because of the limitation of the representable number of bits. Furthermore, as shown in Fig. 1, there are often significant differences in weight ranges across out channels, and relatively narrow-ranged weights in specific channels are quantized to just a few quantized values. This can deteriorate the accuracy in the layer-wise quantization (LWQ) scheme. To address this problem, per-channel bit allocation (Banner, Nahshan, and Soudry 2019) and ZeroQ (Cai et al. 2020) were introduced but mixed precision is more complicated to implement in hardware than homogeneous precision. Most commodity hardwares do not support efficient mixed precision computation due to chip area constraints (Liu et al. 2020). Outlier-channel splitting (Zhao et al. 2019a) minimized quantization error by halving weights belonging to outliers in the distribution and increasing channels. However, this can increase the cost of network size overhead.

In this work, we focus on proposing a straightforward but powerful manner to recover the baseline accuracy in the PTQ scheme.

- To minimize the accuracy drop after PTQ, a shift-based channel-wise weight scaling method is introduced prior to the quantization process. This aligns weight ranges across channels approximately so quantization error is drastically reduced. Inverse binary shifting is efficiently fused to the existing per-layer scale compounding to recover the original output range.

- The proposed work is validated using state-of-the-art

models in varying tasks (image classification, object detection, super-resolution). In particular, we use a large scale dataset such as ImageNet and focus on up-to-date models considering both accuracy and efficiency rather than traditional deep models with high redundancy. Plus, we intactly utilize only open pre-trained models without retraining.

## Previous Works

There are a couple of comparable studies to reduce quantization error using a homogeneous precision level in PTQ. To name representative methods, there are channel-wise quantization (CWQ) (Krishnamoorthi 2018) and data-free quantization (DFQ) (Nagel et al. 2019).

## Pitfalls of Channel-wise Quantization

Layer-wise quantization produces a single set of scale compound and zero point per layer, thus unabling to preserve weight values in the relatively narrow-ranged channels after quantization.

**1. Bigger parameter size:** To address the problem, channel-wise quantization gives as many sets of the parameters as the number of channels. Despite a guarantee of high accuracy, however, the bigger parameter size can be burdensome if deploying the model on edge devices with limited memory resource. That is because it can cause a latency issue due to a delayed loading of the parameters increased per each channel.

**2. Bias overflow:** In addition, the channel-wise scales,  $(max_i - min_i)/(2^{bits} - 1)$ , in depth-wise convolution are sometimes quite small so that as quantizing the bias by the multiplication of the scale of input and scale of weight,  $B^i/(s_{in}s_w^i)$ , it incurs a 32-bit overflow issue in conventional NPU. To prohibit the overflow, the  $[min, max]$  range determining the scale should be forced to be adjusted. That is, if the computed scale is less than the low bound (e.g.,  $1e-5$ ), the max range is extended, fitting to the scale bound. Though, this ad hoc recipe discards the precision gain of channel-wise quantization.

## Pitfalls of Data-free Quantization

To tackle the accuracy drop in the MobileNet family, data-free quantization (Nagel et al. 2019) rescales the weight scales across subsequent layers by making use of a scale-equivariance property of activation functions and the scale factor is searched by an iterative optimization.

**1. Model modification:** However, ReLUN(N=6) requires a different cut off per channel after applying the scale eqlization procedure. Due to hardware complexity, this algorithm supports regular ReLU activation function efficiently. Thus, it requires the replacement of the activation function.

**2. Retraining:** After the architecture change, task accuracy could decrease because of the change of distribution after activation function. In the reference paper, the authors claim little accuracy drop in PyTorch but we experienced nontrivial accuracy degradation (70.60%  $\rightarrow$  55.45%, 71.87%  $\rightarrow$  64.90%) for MobileNet v1/v2 <sup>1</sup> pretrained in Tensorflow

<sup>1</sup><https://github.com/fchollet/deep-learning-models/releases>

Keras. This can depend on the training quality of pre-trained models. To recover the baseline accuracy, further retraining of the changed model using a train dataset is required, however, which is undesirable in post-training quantization.

## Method

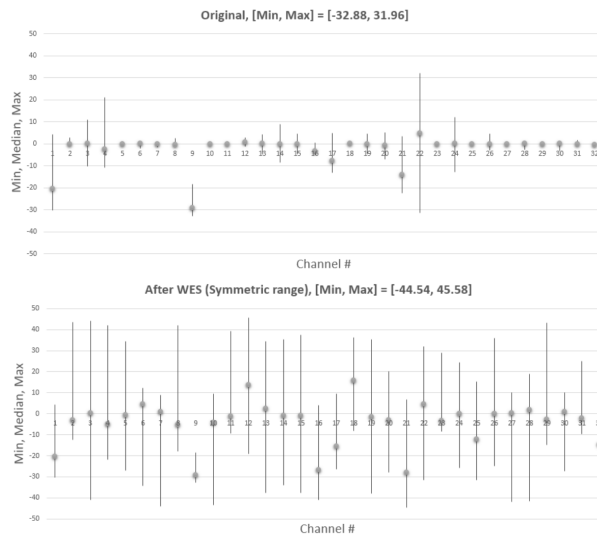


Figure 1: Channel-wise weight ranges and rescaled weight ranges by WES of the 1st depthwise convolutional layer in MobileNet v1. Min, median, and max values are plotted.

## Fundamental of Uniform Affine Quantization

For each layer, quantization is parameterized by the number of quantization levels ( $2^{bit}$ ) and a clamping range ( $a, b$ ), and is performed by applying the element-wise quantization function  $q_w$  defined as follows (Jacob et al. 2018):

$$\text{clamp}[x; a, b] = \min(\max(x, a), b), \quad (1)$$

$$s = \frac{\max - \min}{2^{bits} - 1}, \quad z = \lfloor \frac{-\min}{s_w} \rfloor, \quad (2)$$

$$q = \lfloor \frac{1}{s} (\text{clamp}[w; \min, \max] - \min) \rfloor, \quad (3)$$

where the boundaries  $[min, max]$  are nudged by small amounts so that value 0.0 is exactly representable as an integer zero point,  $z$ , after quantization:  $min \leftarrow s * \lfloor min/s \rfloor$ ,  $max \leftarrow max + s * \lfloor min/s \rfloor - min$ . The function  $\lfloor \cdot \rfloor$  rounds to the nearest integer. The scale,  $s$ , indicates the step size of quantization. Uniform affine quantization is also called asymmetric quantization because the quantized range is fully utilized. We exactly map the min/max values from the float range to the min/max of the quantized range due to the existence of the zero point.

## Weight Equalizing Shift Scaler

The proposed method introduces a new weight equalizing shift scaler (WES)-coupled post training quantization having a new quantized parameter called channel-wise shift

scale and its inverse scalings fusion to a convolutional operator in NPU.

**Initialization of a total range** Rescaling the range of original weights to the optimal range per channel before quantization is required to minimize the quantization error. To do so, convolutional weights and bias first fold its following batch norm (BN) layer (Fig. 2 (a)) since most NPUs basically support BN-folded convolutional operation for speed-up inference. An original range  $r_i$  is defined as a symmetric range, which is a maximum between absolute values of max and min of weights in each channel  $i$ . A total range  $\hat{r}$  is the target range in WES to which all channel-wise ranges in a layer will be fitted. This is initialized as a maximum value over all  $r_i$  in a layer:

$$r_i = 2 * \max(|max_i|, |min_i|), \quad \hat{r} = \max(r_i). \quad (4)$$

An integer format of a channel-wise shift scale factor  $\mathbb{S}_i$  to rescale the original range for  $i$ -th output channel tensor into the total range is

$$\mathbb{S}_i = \lfloor \log_2(\hat{r}/r_i) \rfloor, \quad (5)$$

where a floor function  $\lfloor \cdot \rfloor$  gives the greatest integer less than or equal to input.

**Iterative search for an optimal total range** For more minute investigation of the optimal total range  $\hat{r}$ , we use a fake quantization (quantization followed by dequantization)-based optimization scheme where quantization error is defined as a cost function to be minimized.

The WES-coupled fake quantization process is shown in Algorithm 1. In detail, weights are first channel-wise shifted by  $s_i$  (Line 7 in Algorithm 1), followed by uniform affine layer-wise quantization (FP32→UINT8) and dequantization (UINT8→FP32) process (Line 8-10) as emulating inference-time quantization, and then channel-wise shifted in the reversed direction (Line 11). Lastly, the quantization error can be measured in  $l_2$ -norm between original weights and WES-coupled fake quantized weights so that bigger quantization error can be more penalized (Line 12). Note that the floor and round functions used in the fake quantization process have discontinuities at the integers, for which derivatives may not be known. Thus, we use the heuristic non-linear optimization methods such as NelderMead (Nelder and Mead 1965) or Bayesian optimization (Pelikan et al. 1999) where they iteratively search for the local minima of the cost function while the absolute error between iterations is greater than a tolerance.

**Channel-wise shift scale** Given the optimal channel-wise shift scale  $\mathbb{S}_i$ , the original weights  $w_i$  and bias  $b_i$  are rescaled to  $\hat{w}_i$  and  $\hat{b}_i$  by a shift operation (Line 14 in Algorithm 1):

$$\hat{w}_i = w_i \ll \mathbb{S}_i, \quad \hat{b}_i = b_i \ll \mathbb{S}_i, \quad (6)$$

This WES process shifts the weights closely fitting to the total weight range (Fig. 2 (b)). Next, a scale ( $s_w$ ) and a zero point ( $z_w$ ) are derived by uniform affine layer-wise quantization (Fig. 2 (c)). The scale specifies the step size of the quantizer and the zero point is an integer mapped to the floating point zero value (Krishnamoorthi 2018). In particular, the

distribution of the channel with a relatively narrow range is stretched out so it comes to having low quantization error after WES-coupled quantization. The process so far is performed in compile time and a resultant quantized model is saved to a binary file.

---

**Algorithm 1: Weight equalizing shift scaler (WES)**

---

```

1  $w, b \leftarrow \text{BN\_fold}(w, b, \gamma, \beta, \mu, \sigma^2)$ 
2  $[min_i, max_i] = [\min(w_i), \max(w_i)]$ 
3  $r_i = 2 * \max(|max_i|, |min_i|)$ 
4  $\hat{r} = \max(r_i)$  // initialization of trainable variable
5 while  $|\phi - \phi_{old}| > tol$  do
6    $\mathbb{S}_i = \lfloor \log_2(\hat{r}/r_i) \rfloor$ 
7    $\hat{w}_i = w_i \ll \mathbb{S}_i$ 
8    $[min, max] = [\min(\hat{w}), \max(\hat{w})]$ 
9    $s_w = \frac{max - min}{2^{bits} - 1}$ 
10   $\hat{w}_i^* = s_w * \lfloor \frac{1}{s_w}(\hat{w}_i - min) \rfloor + min$ 
11   $w_i^* = \hat{w}_i^* \gg \mathbb{S}_i$ 
12   $\phi = \frac{1}{n} \sum (w_i - w_i^*)^2$ 
13 end
14  $\hat{w}_i = w_i \ll \mathbb{S}_i \quad \hat{b}_i = b_i \ll \mathbb{S}_i$ 

```

---

## WES-coupled Fixed-point Computing in NPU

In this section, we describe how to implement a convolutional operation, adapting the change by our proposed WES to the fixed-computing NPU. From end to end of network, all the computations are performed in the integer format.

The rescaled output feature maps are resulted from matrix multiplication and vector addition using weights and bias rescaled by WES described in the previous section. Their original output range needs to be recovered before an activation function. To do so, it should be followed by a channel-wise inverse shift scaling,  $s_i^{-1}$  (Fig. 2 (b)). However, it is undesirable to have an additional layer that did not exist in the original model.

To fuse the convolutional layer and the channel-wise inverse shift scaling layer, it is necessary to design a WES-specialized convolutional operator in NPU as shown in Algorithm 2. In order to produce a fixed-point output  $q_{out}$  using given a fixed-point input  $q_{in}$ , the NPU operators take supported integer-format weights  $q_w$  (uint8), and its quantization-related parameters such as scales (float32),  $s_w$ ,  $s_{in}$ ,  $s_{out}$  and zero points (uint8),  $z_w$ ,  $z_{in}$ ,  $z_{out}$ , respectively. There exists a single set of those quantization parameters per each layer in layer-wise quantization. In the fixed-computing convolutional operation (Jacob et al. 2018), the output  $q_{out}^i$  for channel  $i$  is computed by

$$s_{out}(q_{out}^i - z_{out}) = \sigma \left( \sum_j \sum_{h_w, w_w} s_w(q_w^{ij} - z_w) s_{in}(q_{in}^j - z_{in}) + B^i \right). \quad (7)$$

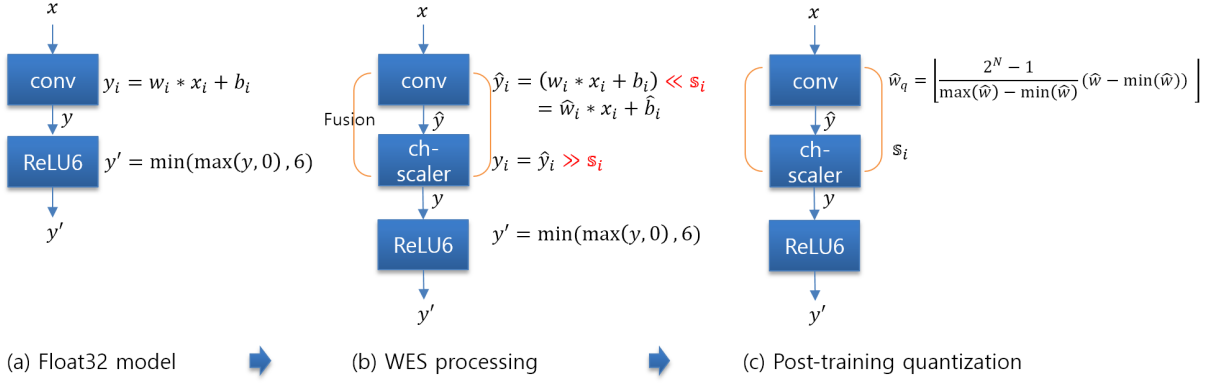


Figure 2: The WES-coupled post-training quantization procedure. Channel-wise shift scale and its inverse scalings fusion to a convolutional operator in the neural processing unit (NPU).

Table 1: Weight parameter specification after layer-wise vs. channel-wise vs. WES-coupled layer-wise quantization.  $M$  and  $s$  are the mantissa and the exponent of a scale compound and the subscript  $i$  denotes a channel index out of  $N$  channels.  $\mathbb{S}_i$  is a channel-wise shift scale. DFQ has the same spec. as LWQ.

Weight params	bits	LWQ	CWQ	WES
	32	$M$	$M_i \times N$	$M$
Scale compound	6	$s$	$s_i \times N$	$s$
	4	-	-	$\mathbb{S}_i \times N$
Zero point	8	$z$	$z_i \times N$	$z$

This can be refactored to

$$q_{out}^i = z_{out} + \sigma \left( \frac{s_{in}s_w}{s_{out}} \left( \left( \sum_j \sum_{h_w, w_w} (q_w^{ij} - z_w)(q_{in}^j - z_{in}) \right) + q_B^i \right) \right), \quad (8)$$

where  $\sigma(\cdot)$  is a piece-wise linear activation function (e.g., ReLU, ReLUN) and  $q_B^i$  denotes the quantized bias through  $B^i/(s_{in}s_w)$ .  $h_w$  and  $w_w$  indicate height and width of a weight tensor, and  $i$  and  $j$  denote indices of output and input channels. A scale compound  $(s_{in}s_w)/s_{out}$  is the same over the channels, and is approximated to a binary floating-point number format with a fixed number of significant digits (mantissa) and scaled using an exponent:  $M * 2^s$ .  $M$  is a 32-bit mantissa representing a value in the interval  $[0.5, 1)$  and  $s$  is a 6-bit integer-format exponent, enabling a shift in the left or right direction.

Herein, we can incorporate an inversion of channel-wise shift scale,  $\mathbb{S}_i^{-1}$ , by simply shifting the binary floating-point number by  $\mathbb{S}_i$  to the right direction (Line 21 in Algorithm 2). Based on our experiments, 4 bits are enough to represent the candidates of channel-wise shift scales,  $2^{\mathbb{Z}}$ ,  $\mathbb{Z} \in \{0, \dots, 15\}$ . This binary shift is a key feature, which improves the accuracy performance without harming the latency due to a hardware-friendly bit-wise operation. The major scale com-

**Algorithm 2:** WES-coupled fixed-point computing operator of Conv + ReLU (or ReLUN)

---

```

1 input and its zero point:  $q_{in}, z_{in}$ 
2 output's zero point:  $z_{out}$ 
3 weights and its zero point:  $q_w, z_w$ 
4 bias:  $q_B$ 
5 scale compound of  $\{s_{in}, s_w, s_{out}\} \rightarrow M, s$ 
6 ch-wise shift scale:  $\mathbb{S}_i$ 
7 for  $0 \leq x < w_{out}, 0 \leq y < h_{out}, 0 \leq z < c_{out}$  do
8    $acc_{32} = 0$ 
9    $ix_- = x * stride - pad_{left}$ 
10   $iy_- = y * stride - pad_{top}$ 
11  for  $0 \leq i < w_w, 0 \leq j < h_w$  do
12     $ix = ix_- + i$ 
13     $iy = iy_- + j$ 
14    if  $0 \leq ix < w_{in}, 0 \leq iy < h_{in}$  then
15      for  $0 \leq k < c_{in}$  do
16         $acc_{32} += (int32)((int16)q_{in}[iy * w_{in} * c_{in} + ix * c_{in} + i] - (int16)z_{in}) * ((int16)q_w[j * w_w * c_{in} * c_{out} + i * c_{in} * c_{out} + k * c_{out} + z] - (int16)z_w)$ 
17      end
18    end
19  end
20   $acc_{32} += q_B[z]$ 
21   $out_{32} = M * (((s > 0)?(out_{32} \ll s) : (out_{32} \gg -s)) \gg \mathbb{S}_{i=z})$ 
22   $out_{32} = (relu)?max(0, out_{32}) : out_{32}$ 
23   $out_{32} += z_{out}$ 
24   $outs_8[y * w_{out} * c_{out} + x * c_{out} + z] = sat\_uint8(out_{32})$ 
25 end
```

---

pound and zero point are shared across channels, and furthermore the shift scale adjusts the range per channel, which is very cost-effective. Table 1 shows the difference of quantization parameter specification among LWQ, CWQ, and WES.

## Experimental Results

We validate our proposed WES quantization method using up-to-date models in varying tasks compared to previous methods. We quantize only open models that already completed training.

### Baseline Methods

Our interest is confined to uniform affine (with a zero point) quantization, which is known for its hardware-friendliness and fundamental needs. As representative methods to tackle the accuracy degradation after post-training quantization, channel-wise quantization (CWQ), and data-free quantization (DFQ) are the target baseline methods that our WES is compared to. Besides, layer-wise quantization (LWQ) is also included for the ablation study of WES.

### Experimental Setup

The computing environment is Python 3.7, Tensorflow (TF) 2.0 with a single GPU P40. The pre-trained models that are officially referred to in TF or are popularly cited are downloaded and we do not fine-tune the model. All convolutional layers including a depth-wise convolution and a fully-connected layer are quantized. For activation quantization, 1K representative images are selected at random in a train dataset but the label information is not used. Also, we do not make use of validation accuracy estimation in a cost or loss function. The result using DFQ was reproduced in our TF code migrated from PyTorch code<sup>2</sup>. For fair comparison, the activation ranges were safely set by feeding representative data, not predicting ranges from the batch normalization parameters ( $\beta, \gamma$ ) proposed in DFQ.

**Weight clipping:** In uniform (or linear) quantization, quantization error is bounded by a half of the quantization step or scale which increments as the dynamic range increases (Gibson et al. 1998). Assuming that weights can lie on the long-tailed distribution, the weight values outside a fixed interval are clipped to the interval edges. This leads to an increase in clipping error but a decrease in quantization error, so it is important to find the optimal range to make a balance between the errors. This clipping process is performed after the WES process just before layer-wise quantization. The reason is that some depth-wise weights in MobileNet before WES processing tend to be congregated in the narrow and distant range (Fig. 1) in specific channels. To disperse the clipping evenly to other channels, it is recommended to apply the weight clipping after WES rescales weights. To find the optimal clipping range per layer, we use a heuristic non-linear optimization method (NelderMead) where the cost is defined as the sum of clipping error and quantization error.

**Weight pruning:** To take advantage of weight sparsification, the pruning technique (Zhu and Gupta 2017) can be applied prior to the WES process. In NPU, this can help reduce DRAM bandwidth and SRAM size, thereby increasing power efficiency (FPS/W) without significantly compromising accuracy. To prune weights, the magnitude threshold is empirically set up. Then, unimportant elements, which have the magnitude of the weight value less than the threshold, are nullified to zero. The sparse weights are compressed by representing them as 1-bit masks with the same dimension of the original weights, compactly packed non-zero weights, and a single integer indicating the size of the compressed data.

**Activation quantization:** For activation quantization, layer-wise quantization is applied. Variants of convolution operator (e.g., normal, depthwise) and followed piece-wise linear activation function (e.g., ReLU, ReLU6) are fused for speeding-up inference and reducing fixed-computing error caused by the scaling and the datatype conversion. The dynamic range  $[min, max]$  after activation function is obtained in the statistical way. In specific, we obtain min's and max's distributions by feeding representative images without labels to the network model and then the final  $[min, max]$  is determined as the left and right clipping edges corresponding to the fixed percentile (1%) in each distribution, respectively.

### Applications

**Image classification:** The ImageNet Large Scale Visual Recognition Challenge (ILSVRC) 2012 (Deng et al. 2009; Russakovsky et al. 2015) is a large visual database, containing 1K sub-classes, 1.2M images as training dataset and 50K images as evaluation dataset. We choose various backbone models targeting ImageNet classification from mobile-oriented light models to cloud-oriented heavy models such as MobileNet v1/v2 (Howard et al. 2017; Sandler et al. 2018), EfficientNet B0/B3 (Tan and Le 2019), ResNet50 (He et al. 2016), and Inception v3 (Szegedy et al. 2016). Only when applying DFQ to the MobileNet family, ReLU6 is replaced with ReLU due to the algorithm constraint, which is then finetuned for 40 epochs with 1e-5 initial learning rate. Otherwise, original pre-trained models are quantized.

CIFAR-10 (Torralba, Fergus, and Freeman 2008) is a tiny image dataset that is a collection of 32x32 colour images in 10 classes, with 6K images per class. We employ ResNet56 that is a model trained on CIFAR-10 dataset.

**Multiple object detection:** Localization and identification of multiple objects in images is a more advanced topic than image classification. Single shot multibox detection (SSD) (Liu et al. 2016) eliminates miscellaneous processes and encapsulates all computation in a single network. Owing to these features, SSD is known for being faster and more accurate than previous YOLO (Redmon et al. 2016) or Faster R-CNN (Ren et al. 2015) networks. Replacing the backbone network, VGG16, of SSD with effective MobileNet v1 invented the state-of-the-art modern object detection system, MobileNet-SSD (Howard et al. 2017), which is pre-trained on the Widerface dataset (Yang et al. 2016) for the face detection benchmark.

<sup>2</sup><https://github.com/jakc4103/DFQ>

**Super resolution:** Image super-resolution (SR) has been focused in the image processing area since the advent of deep learning. Fast Super-Resolution Convolutional Neural Networks (FSRCNN) (Dong, Loy, and Tang 2016) is one of well-known SR networks achieving both of accuracy and speed. The model is pre-trained on 91-images and is tested on Set14.

### Ablation Study

In this section we explore the effect of our WES method on the image classification task. It is validated on MobileNet v1/v2 and EfficientNet B3 using ImageNet validation dataset. We assume the accuracy degradation arises from varying ranged and small overlapped distribution of weights across channels. To measure the difference and effect of the overlapping of LWQ and WES, a new metric, a so-called overlap ratio, is defined as follows:

$$\text{Overlap ratio} = \frac{1}{N} \sum_{i=1}^N \frac{\max_i - \min_i}{\max - \min}, \quad (9)$$

where  $[\min_i, \max_i]$  is a weight range of  $i$ -th channel and  $[\min, \max]$  is a range of all  $N$  channels, i.e. the minimum of  $\min_i$  and the maximum of  $\max_i$ . Besides, quantization error is measured in the fake quantization procedure and test accuracy is estimated using test dataset after UINT8 weight and activation quantizations.

As illustrated in Fig. 3, WES shows significant improvement ( $2 \sim 3\times$ ) in the overlap ratio over the baseline LWQ. The improvement is observed evenly in all the depth-wise and normal convolution layers. In the MobileNet and EfficientNet families including MBConv (Sandler et al. 2018; Tan and Le 2019) block, the effect of WES is outstanding. Accordingly, the quantization error is reduced as much as  $3 \sim 12\times$ , which results in the accuracy recovery close to the FP32 base model (70.60% vs. 69.68%, 71.87% vs. 69.73%, 81.38% vs. 80.14%). This ablation study proves the success of WES in that independent weight shift scaling per channel is straightforward but very effective in greatly improving the precision of per-layer quantization. We also experimented that WES is applied to only depth-wise convolution layers while applying LWQ to normal convolution layers. This is because we considered reusing the most of existing LWQ-based fixed-computing operators but the depth-wise convolutions. The partial application of WES to the depth-wise convolutions yields the insufficient accuracy gain, 69.68%  $\rightarrow$  63.16% in MobileNet v1. Thus, overall improvement of the range overlap in all convolution layers is important to achieve the best accuracy.

The iterative search was introduced for finding an optimal total range in Algorithm 1. The initial value of the variable is determined with a maximum value over all channel-wise ranges (deterministic). The iterative search based on the Nelder-Mead heuristic non-linear optimization further refines the variable (iterative). In order to confirm the effect of iterative search, we compare the performance resulted from the iterative search versus the deterministic way. Table 2 shows that the iterative search helps further improve the overlap ratio, reduce the quantization error, and increase the

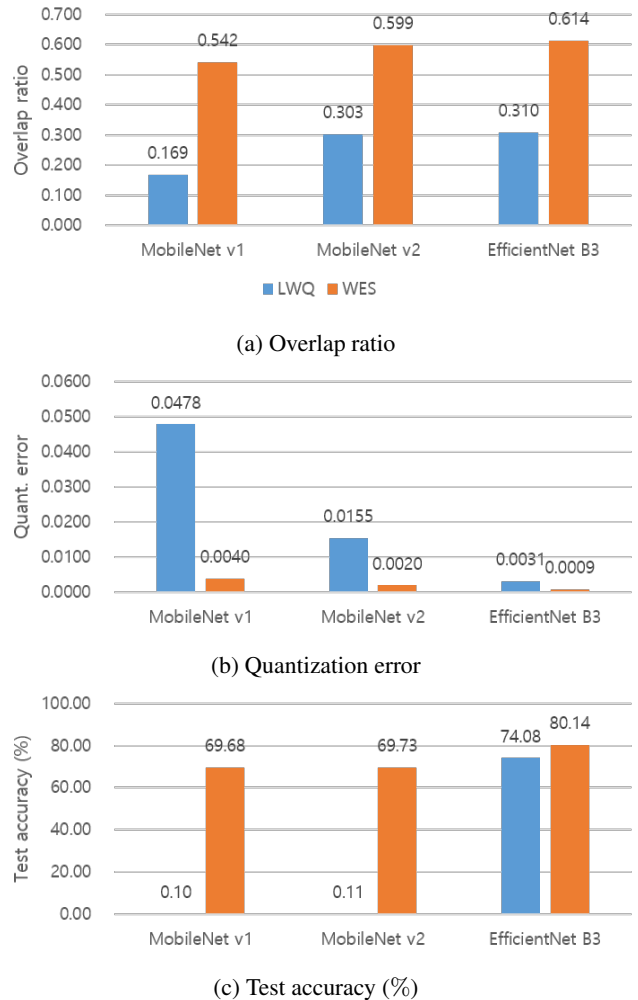


Figure 3: Ablation study of WES (orange) compared to LWQ (blue) in perspectives of overlap ratio, quantization error, and test accuracy.

test accuracy (69.5%  $\rightarrow$  69.7%) in MobileNet v1. Note that if the quantization error is small enough, albeit that there exists slight improvement in quantization error, it always does not guarantee better test accuracy like MobileNet v2.

### Comparison to Other Methods and Applications

The performance of WES is compared with LWQ, DFQ (Nagel et al. 2019), and CWQ in various application domains including image classification, object detection and super-resolution. Table 3 summarizes the post-training quantization results in UINT8. For MobileNet v1/v2, the results applying weight clipping with a fixed percentile are also shown.

In detail, WES outperforms DFQ for MobileNet v1 (69.78% vs. 67.52%) and MobileNet v2 (70.96% vs. 69.12%) in accuracy. DFQ employs bias correction in addition to cross-layer equalization so as to correct for the biased quantization error in the bias. Nevertheless, our reproduced

Table 2: Deterministic or iterative search of an optimal total range in MobileNet v1/v2. We report the test accuracy just with weight quantization to exclude the random effect by data shuffling in activation quantization.

	Overlap Ratio	Quant. Error	Test Acc. (%)
<b>MobileNet v1</b>			
Deterministic	0.535	0.00402	69.5
Iterative	0.542	0.00398	69.7
<b>MobileNet v2</b>			
Deterministic	0.586	0.00202	69.8
Iterative	0.599	0.00199	69.8

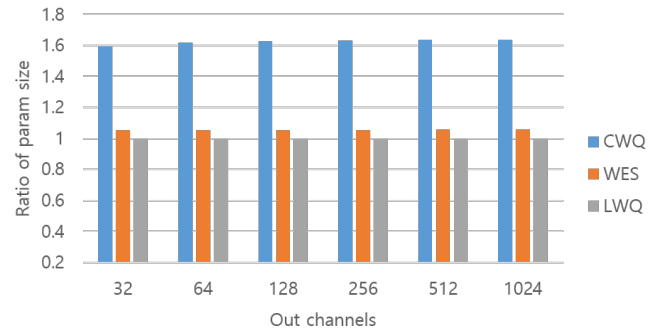
results are similar to or worse than ones without bias correction.

In general, it is shown that WES is very competitive to CWQ in all the target applications in this paper. CWQ shows slightly better performance over WES in MobileNet v1 (69.97% vs. 69.78%), MobileNet v2 (70.98% vs. 70.96%), and EfficientNet (80.20% vs. 80.14%) containing depth-wise convolution layers. However, WES gives better or similar performance in the other models – ResNet50 v1 (76.29% vs. 76.20%), Inception v3 (77.64% vs. 77.61%), ResNet56 (93.29% vs. 93.18%), FSRCNN (30.64dB vs. 30.59dB) than CWQ. Carefully speaking, based on our experiments, the proposed WES method proves its robust performance in varying applications.

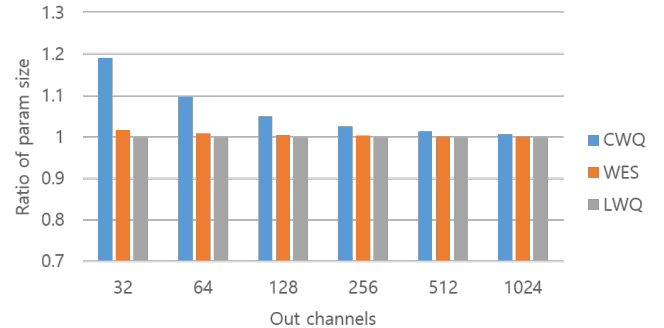
## Memory Cost

With respect to the size of quantized parameters, WES needs just extra 4 bits for storing shift scale factor for each channel, on the other hand, CWQ needs a (32+6)-bit scale compound, a 8-bit zero point of weights for each channel. As shown in Fig. 4 (a), in 3x3 depth-wise convolution, WES slightly increases by 5.5%, but CWQ increases by 59% ~ 64% compared to LWQ consistently over the number of channels. By contrast, in normal convolution, the difference of CWQ or WES against LWQ in size is negligible because kernel weights occupy much larger portion out of the overall than depth-wise convolution. Table 4 shows the overall size of naive quantized parameters without weight compression. For CWQ, parameter increment of around 3% incurs but for WES around 0.2%.

If we further compress pruned weights into a sparse format, the advantage of WES saving the quantization parameters is clearly present in normal convolution as Fig. 4 (b). The benefit of WES is shown differently depending on the number of channels. For example, applying a sparsity of 20% by weight compression is shown to preserve the accuracy within 1% drop. The parameter size increases by 0.1% to 1.7% for 32 to 1024 channels in WES but by 0.6% to 19.1% in CWQ compared to LWQ. As the sparsity gets bigger, the effect will be larger.



(a)



(b)

Figure 4: Quantized parameter size of (a) 3x3 depth-wise convolution and (b) 1x1 point-wise convolution for LWQ, CWQ, and WES for different number of channels. A sparsity of 20% by weight pruning is assumed in 1x1 point-wise convolution.

## Conclusion

We addressed the accuracy degradation problem after quantizing weights of a varying distribution per channel in layer-wise quantization. The proposed method introduced a new weight equalizing shift scaler (WES)-coupled post training quantization having a new quantized parameter called channel-wise shift scale and its inverse scalings fusion to a convolutional operator in the neural processing unit (NPU). This method significantly improved the accuracy performance without harming the memory footprint. The ablation and experimental study showed that WES can successfully resolve the accuracy degradation problem of layer-wise quantization. In addition, its robust performance was proved over varying applications.

## Future Works

As future works, we will measure the system cycle for WES and baseline methods in the simulator environment of our custom-designed NPU. For automating the decision of the optimal pruning percentile for weight compression, optimization-based method will be tried. Other than vision tasks, we will expand validation to language tasks like acoustic speech recognition or natural language understanding.

Table 3: Accuracy of post-training quantization (UINT8). The symbol <sup>wc</sup> denotes the result from additional application of weight clipping. The clipping range is optimized using a heuristic non-linear optimization method (See the details in the section of Experimental Setup).

Dataset	Model	Accuracy	Baseline (FP32)	LWQ	CWQ	DFQ	WES
ImageNet	MobileNet v1	Top1(%)	70.60	0.10	69.74 / <b>69.97<sup>wc</sup></b>	66.67 / 67.52 <sup>wc</sup>	69.68 / 69.78 <sup>wc</sup>
	MobileNet v2	Top1(%)	71.87	0.11	70.98 / <b>70.98<sup>wc</sup></b>	69.12	69.73 / 70.96 <sup>wc</sup>
	EfficientNet B3	Top1(%)	81.38	74.08	<b>80.20</b>	-	80.14
	ResNet50 v1	Top1(%)	76.48	76.18	76.20	-	<b>76.29</b>
	Inception v3	Top1(%)	77.97	77.62	77.61	-	<b>77.64</b>
Cifar10	ResNet56	Top1(%)	93.37	93.28	93.18	-	<b>93.29</b>
Widerface	MobileNet-SSD	mAP(%)	54.29	52.32	<b>55.20</b>	-	55.05
91Im/Set14	FSRCNN	PSNR(dB)	30.79	30.62	30.59	-	<b>30.64</b>
		SSIM	0.898	0.893	0.893	-	<b>0.894</b>

Table 4: Quantized parameter size (MB) of post-training quantization (UINT8) without weight compression

Dataset	Model	Baseline (FP32)	LWQ / DFQ	CWQ	WES
ImageNet	MobileNet v1	16.5	4.16	4.22	4.16
	MobileNet v2	13.7	3.46	3.56	3.47
	EfficientNet B3	47.8	12.10	12.46	12.13
	ResNet50 v1	99.8	25.0	25.2	25.0
	Inception v3	93.0	23.3	23.4	23.3

## Acknowledgement

This work is supported by Samsung Research, Samsung Electronics Co.Ltd.

## References

- Albericio, J.; Delmás, A.; Judd, P.; Sharify, S.; O’Leary, G.; Genov, R.; and Moshovos, A. 2017. Bit-pragmatic deep neural network computing. In *Proceedings of the 50th Annual IEEE/ACM International Symposium on Microarchitecture*, 382–394.
- Banner, R.; Nahshan, Y.; and Soudry, D. 2019. Post training 4-bit quantization of convolutional networks for rapid-deployment. In *Advances in Neural Information Processing Systems*, 7950–7958.
- Cai, Y.; Yao, Z.; Dong, Z.; Gholami, A.; Mahoney, M. W.; and Keutzer, K. 2020. Zeroq: A novel zero shot quantization framework. In *Proceedings of the IEEE/CVF Conference on Computer Vision and Pattern Recognition*, 13169–13178.
- Chen, Y.-H.; Emer, J.; and Sze, V. 2016. Eyeriss: A spatial architecture for energy-efficient dataflow for convolutional neural networks. *ACM SIGARCH Computer Architecture News* 44(3): 367–379.
- Courbariaux, M.; Bengio, Y.; and David, J.-P. 2015. Binaryconnect: Training deep neural networks with binary weights during propagations. In *Advances in neural information processing systems*, 3123–3131.
- Deng, J.; Dong, W.; Socher, R.; Li, L.-J.; Li, K.; and Fei-Fei, L. 2009. Imagenet: A large-scale hierarchical image database. In *2009 IEEE conference on computer vision and pattern recognition*, 248–255. Ieee.
- Dong, C.; Loy, C. C.; and Tang, X. 2016. Accelerating the super-resolution convolutional neural network. In *European conference on computer vision*, 391–407. Springer.
- Gibson, J. D.; Berger, T.; Lookabaugh, T.; Baker, R.; and Lindbergh, D. 1998. *Digital compression for multimedia: principles and standards*. Morgan Kaufmann.
- Han, S.; Mao, H.; and Dally, W. J. 2015. Deep compression: Compressing deep neural networks with pruning, trained quantization and huffman coding. *arXiv preprint arXiv:1510.00149*.
- He, K.; Zhang, X.; Ren, S.; and Sun, J. 2016. Deep residual learning for image recognition. In *Proceedings of the IEEE conference on computer vision and pattern recognition*, 770–778.
- Horowitz, M. 2014. 1.1 computing’s energy problem (and what we can do about it). In *2014 IEEE International Solid-State Circuits Conference Digest of Technical Papers (ISSCC)*, 10–14. IEEE.
- Howard, A. G.; Zhu, M.; Chen, B.; Kalenichenko, D.; Wang, W.; Weyand, T.; Andreetto, M.; and Adam, H. 2017. Mobilenets: Efficient convolutional neural networks for mobile vision applications. *arXiv preprint arXiv:1704.04861*.
- Hubara, I.; Courbariaux, M.; Soudry, D.; El-Yaniv, R.; and Bengio, Y. 2016. Binarized neural networks. In *Advances in neural information processing systems*, 4107–4115.

- Jacob, B.; Kligys, S.; Chen, B.; Zhu, M.; Tang, M.; Howard, A.; Adam, H.; and Kalenichenko, D. 2018. Quantization and training of neural networks for efficient integer-arithmetic-only inference. In *Proceedings of the IEEE Conference on Computer Vision and Pattern Recognition*, 2704–2713.
- Jouppi, N. P.; Young, C.; Patil, N.; Patterson, D.; Agrawal, G.; Bajwa, R.; Bates, S.; Bhatia, S.; Boden, N.; Borchers, A.; et al. 2017. In-datacenter performance analysis of a tensor processing unit. In *Proceedings of the 44th Annual International Symposium on Computer Architecture*, 1–12.
- Judd, P.; Albericio, J.; Hetherington, T.; Aamodt, T. M.; and Moshovos, A. 2016. Stripes: Bit-serial deep neural network computing. In *2016 49th Annual IEEE/ACM International Symposium on Microarchitecture (MICRO)*, 1–12. IEEE.
- Jung, S.; Son, C.; Lee, S.; Son, J.; Han, J.-J.; Kwak, Y.; Hwang, S. J.; and Choi, C. 2019. Learning to quantize deep networks by optimizing quantization intervals with task loss. In *Proceedings of the IEEE Conference on Computer Vision and Pattern Recognition*, 4350–4359.
- Krishnamoorthi, R. 2018. Quantizing deep convolutional networks for efficient inference: A whitepaper. *arXiv preprint arXiv:1806.08342*.
- Lee, D.; Kapoor, P.; and Kim, B. 2018. Deeptwist: Learning model compression via occasional weight distortion. *arXiv preprint arXiv:1810.12823*.
- Lee, J.; Kim, C.; Kang, S.; Shin, D.; Kim, S.; and Yoo, H.-J. 2018. UNPU: A 50.6 TOPS/W unified deep neural network accelerator with 1b-to-16b fully-variable weight bit-precision. In *2018 IEEE International Solid-State Circuits Conference-(ISSCC)*, 218–220. IEEE.
- Liu, W.; Anguelov, D.; Erhan, D.; Szegedy, C.; Reed, S.; Fu, C.-Y.; and Berg, A. C. 2016. Ssd: Single shot multibox detector. In *European conference on computer vision*, 21–37. Springer.
- Liu, X.; Ye, M.; Zhou, D.; and Liu, Q. 2020. Post-training Quantization with Multiple Points: Mixed Precision without Mixed Precision. *arXiv preprint arXiv:2002.09049*.
- Nagel, M.; Baalen, M. v.; Blankevoort, T.; and Welling, M. 2019. Data-free quantization through weight equalization and bias correction. In *Proceedings of the IEEE International Conference on Computer Vision*, 1325–1334.
- Nelder, J. A.; and Mead, R. 1965. A simplex method for function minimization. *The computer journal* 7(4): 308–313.
- Pelikan, M.; Goldberg, D. E.; Cantú-Paz, E.; et al. 1999. BOA: The Bayesian optimization algorithm. In *Proceedings of the genetic and evolutionary computation conference GECCO-99*, volume 1, 525–532. Citeseer.
- Redmon, J.; Divvala, S.; Girshick, R.; and Farhadi, A. 2016. You only look once: Unified, real-time object detection. In *Proceedings of the IEEE conference on computer vision and pattern recognition*, 779–788.
- Ren, S.; He, K.; Girshick, R.; and Sun, J. 2015. Faster r-cnn: Towards real-time object detection with region proposal networks. In *Advances in neural information processing systems*, 91–99.
- Russakovsky, O.; Deng, J.; Su, H.; Krause, J.; Satheesh, S.; Ma, S.; Huang, Z.; Karpathy, A.; Khosla, A.; Bernstein, M.; et al. 2015. Imagenet large scale visual recognition challenge. *International journal of computer vision* 115(3): 211–252.
- Sandler, M.; Howard, A.; Zhu, M.; Zhmoginov, A.; and Chen, L.-C. 2018. Mobilenetv2: Inverted residuals and linear bottlenecks. In *Proceedings of the IEEE conference on computer vision and pattern recognition*, 4510–4520.
- Szegedy, C.; Vanhoucke, V.; Ioffe, S.; Shlens, J.; and Wojna, Z. 2016. Rethinking the inception architecture for computer vision. In *Proceedings of the IEEE conference on computer vision and pattern recognition*, 2818–2826.
- Tan, M.; and Le, Q. V. 2019. Efficientnet: Rethinking model scaling for convolutional neural networks. *arXiv preprint arXiv:1905.11946*.
- Torralba, A.; Fergus, R.; and Freeman, W. T. 2008. 80 million tiny images: A large data set for nonparametric object and scene recognition. *IEEE transactions on pattern analysis and machine intelligence* 30(11): 1958–1970.
- Yang, S.; Luo, P.; Loy, C. C.; and Tang, X. 2016. WIDER FACE: A Face Detection Benchmark. In *IEEE Conference on Computer Vision and Pattern Recognition (CVPR)*.
- Zhao, R.; Hu, Y.; Dotzel, J.; De Sa, C.; and Zhang, Z. 2019a. Improving neural network quantization without retraining using outlier channel splitting. *arXiv preprint arXiv:1901.09504*.
- Zhao, X.; Wang, Y.; Cai, X.; Liu, C.; and Zhang, L. 2019b. Linear Symmetric Quantization of Neural Networks for Low-precision Integer Hardware. In *International Conference on Learning Representations*.
- Zhu, M.; and Gupta, S. 2017. To prune, or not to prune: exploring the efficacy of pruning for model compression. *arXiv preprint arXiv:1710.01878*.